Scattering properties of polluted dust in 1.6-μm wavelength*

Fan Meng(范 萌)[a)b)], Chen Liang-Fu(陈良富)[a)†], Li Shen-Shen(李莘莘)[a)c)], Tao Jin-Hua(陶金花)[a)], Su Lin(苏 林)[a)], and Zou Ming-Min(邹铭敏)[a)]

[a)] *State Key Laboratory of Remote Sensing Science, Institute of Remote Sensing and Digital Earth, Chinese Academy of Sciences. Beijing* 100101, *China*

[b)] *University of Chinese Academy of Sciences, Beijing* 100049, *China*

[c)] *Rollins School of Public Health, Emory University, Atlanta, GA* 30322, *USA*

(Received 6 October 2013; revised manuscript received 18 February 2014; published online 10 August 2014)

Three typical polluted dust particles (i.e., single coated dust, two-sphere/spheroid system, and coated dust with aggregate) including internal and semi-external mixtures are modeled, and their scattering properties at 1.6-μm wavelength are calculated by using the generalized multi-sphere Mie-solution (GMM) method. We investigate the influences of particle size, morphology, and chemical composition on the scattering parameters of polluted dust particles. The analysis results demonstrate that the single scattering albedo of coated dust is much smaller than that of pure dust, especially for the spheroidal black carbon (BC) coated dust. When a dust particle semi-mixes with another aerosol particle to form a two-sphere/spheroid system, its scattering properties are much more sensitive to the size and species of monomers than the monomer shape. If an aggregated BC attaches to the coated dust, the scattering properties of whole particle mainly depend on the host particle (coated dust).

Keywords: scattering properties, polluted dust, generalized multi-sphere Mie solution method

PACS: 42.25.Fx, 42.68.–w, 92.60.Mt **DOI:** 10.1088/1674-1056/23/10/104203

1. Introduction

Satellite observations of CO_2 concentrations have significantly improved our understanding of climate change.[1] However, the multiple scattering of aerosols, which affects the optical path through the atmosphere, can introduce large uncertainties in CO_2 retrieval when using the weak absorption CO_2 band around 1.6 μm.[2] The rapid economic growth and associated increase in fossil fuel consumption in China have caused a steady increase in particle concentrations, resulting in more frequent hazy days. The brownish haze consists of a mixture of anthropogenic pollution particles such as sulfate, nitrate, organics, black carbon (BC), and organic carbon (OC), together with natural aerosols such as mineral dust.[3,4] Therefore, the accurate CO_2 retrieval using 1.6-μm band, particularly in China, needs the appropriate estimation of the scattering properties for the polluted dust.

When dust particles access regions with heavy anthropogenic emissions, they usually mix with local polluted particles (e.g. BC and OC) and/or uptake of secondary aerosol species (e.g. water-soluble (WS) material).[5] Such internal and semi-external mixing states could change the scattering properties of original dust particles by changing their chemical and morphological properties. The scattering parameters of non-spherical particles can be calculated by the T-matrix method,[6] the finite difference time domain method,[7] and the discrete dipole approximation method.[8] Xu and Gustafson developed the generalized multi-sphere Mie-solution (GMM) method to compute the scattering properties of aggregates. And they made the GMM method suitable for aggregates with irregularly coated monomers by combining the core-mantle sphere Mie theory and the T-matrix method.[9]

In this paper, according to previous transmission electron microscopy (TEM) studies of morphological and chemical characteristics of the polluted dust,[10–12] we model mixed dust and classify them as three typical groups. Group I is defined as individual dust coated with BC, OC or WS. Group II is dust semi-externally mixed with single BC, OC or WS particle, and group III is OC/WS-coated dust semi-externally mixed with aggregated BC. Then their scattering properties are computed by using the GMM method.

2. Methods and models

2.1. GMM method

By combining the core-mantle sphere Mie theory and T-matrix method, the GMM method can provide a strict solution for the scattering problems of aggregates with irregularly core-mantle monomers (e.g. group II and III particles), and also single coated particles with irregular shapes (e.g. group I particles). There are four key steps. (i) The scattered, internal, and incident electromagnetic fields are expanded in terms of spherical vector wave functions. (ii) The partial scattered field at each monomer in the aggregate is formed, and

*Project supported by the Key Program of the National Natural Science Foundation of China (Grant No. 41130528) and the National Basic Research Program of China (Grant No. 2010CB950801).

†Corresponding author. E-mail: chenlf@radi.ac.cn

© 2014 Chinese Physical Society and IOP Publishing Ltd

a large-dimensional linear system derived from the boundary condition is established. (iii) The addition theorem is used to transform the waves scattered by an individual monomer into the incident waves of other monomers of the aggregate. (iv) The scattering interactive coefficients in the linear system are solved by an asymptotic iteration method. The exact expressions of the amplitude scattering matrix elements, cross sections, and asymmetry parameter were given by Xu and Gustafson.[9] The scattering matrix elements are used for calculating the scattering phase function. The total extinction cross section $C_{\rm ext}$, scattering cross section $C_{\rm sca}$, and asymmetry parameter g of an aggregated particle can be expressed as

$$C_{\rm ext} = \frac{4\pi}{k^2}\sum_{l=1}^{L}\sum_{n=1}^{N^l}\sum_{m=-n}^{n} n(n+1)(2n+1)\frac{(n-m)!}{(n+m)!} \times {\rm Re}\left(p_{mn}^{l*}a_{mn}^{l}+q_{mn}^{l*}b_{mn}^{l}\right), \quad (1)$$

$$C_{\rm sca} = \frac{4\pi}{k^2}\sum_{l=1}^{L}\sum_{j=1}^{L}\sum_{n=1}^{N}\sum_{m=-n}^{n}\sum_{v=1}^{N^j}\sum_{u=-v}^{v} n(n+1)(2n+1)\frac{(n-m)!}{(n+m)!} \times {\rm Re}\left[\left(a_{mn}^{l*}a_{uv}^{j}+b_{mn}^{l*}b_{uv}^{j}\right)\widetilde{A}_{mnuv}^{jl} + \left(a_{mn}^{l*}b_{uv}^{j}+b_{mn}^{l*}a_{uv}^{j}\right)\widetilde{B}_{mnuv}^{jl}\right], \quad (2)$$

$$g = \frac{4\pi}{k^2 C_{\rm sca}}\sum_{l=1}^{L}\sum_{j=1}^{L}\sum_{n=1}^{N}\sum_{m=-n}^{n}\sum_{v=1}^{N^j}\sum_{u=-v}^{v} \times n(n+1)(2n+1)\frac{(n-m)!}{(n+m)!} \times {\rm Re}\left[\left(a_{mn}^{l*}a_{uv}^{j}+b_{mn}^{l*}b_{uv}^{j}\right)\widetilde{S}_{mnuv}^{jl} \times \left(a_{mn}^{l*}b_{uv}^{j}+b_{mn}^{l*}a_{uv}^{j}\right)\widetilde{T}_{mnuv}^{jl}\right], \quad (3)$$

where

$$\widetilde{S}_{mnuv}^{jl} = \frac{m}{n(n+1)}\widetilde{B}_{mnuv}^{jl}+\frac{(n+2)(n-m+1)}{(n+1)(2n+1)}\widetilde{A}_{mn+1uv}^{jl} + \frac{(n-1)(n+m)}{n(2n+1)}\widetilde{A}_{mn-1uv}^{jl}, \quad (4)$$

$$\widetilde{T}_{mnuv}^{jl} = \frac{m}{n(n+1)}\widetilde{A}_{mnuv}^{jl}+\frac{(n+2)(n-m+1)}{(n+1)(2n+1)}\widetilde{B}_{mn+1uv}^{jl} + \frac{(n-1)(n+m)}{n(2n+1)}\widetilde{B}_{mn-1uv}^{jl}, \quad (5)$$

a_{mn}^{l} and b_{mn}^{l} are partial scattering coefficients of the l-th monomer, p_{mn}^{l} and q_{mn}^{l} are the incident-field expansion coefficients, $\widetilde{A}_{mnuv}^{jl}$ and $\widetilde{B}_{mnuv}^{jl}$ are vector translation coefficients based on the spherical Bessel function of the first kind, and absorption cross section $C_{\rm abs}$ and single scattering albedo ω can be written as $C_{\rm abs}=C_{\rm ext}-C_{\rm sca}$ and $\omega=C_{\rm sca}/C_{\rm ext}$ respectively.

During the above calculation, the T-matrix method can be introduced to calculate T matrices of irregular monomers in the overall particle reference system. For each individual monomer, owing to the linearity of Maxwell's equations and boundary conditions, the partial scattering coefficients can be expressed in terms of the primary expansion coefficient of the incident field and the particle-centered T-matrix elements as follows:

$$a_{mn}^{l} = \sum_{j=1}^{L}\exp({\rm i}kZ^{j})\sum_{v=1}^{N^j}\sum_{u=-v}^{v}\left(T_{mnuv}^{jl11}p_{uv}+T_{mnuv}^{jl12}q_{uv}\right), \quad (6)$$

$$b_{mn}^{l} = \sum_{j=1}^{L}\exp\left({\rm i}kZ^{j}\right)\sum_{v=1}^{N^j}\sum_{u=-v}^{v}\left(T_{mnuv}^{jl21}p_{uv}+T_{mnuv}^{jl22}q_{uv}\right), \quad (7)$$

where k is the wave number, T_{mnuv}^{jl11}, T_{mnuv}^{jl12}, T_{mnuv}^{jl21}, and T_{mnuv}^{jl22} represent the elements of $\boldsymbol{T}^{jl}$, which is the pivotal quantity in the T-matrix formulation of GMM. And the explicit expressions for the above-mentioned scattering quantities in terms of the particle-centered T-matrix are also derived by Xu and Gustafson.[9] Moreover, the core-mantle sphere Mie theory can extend the GMM method to heterogeneous monomers with core–shell structures.

2.2. Generation of fractal-like aggregates

During the haze event, transported dust is commonly semi-mixed with BC particles formed due to biomass burning and coal combustion. BC particles are always aggregates composed of ten to hundreds of tiny and nearly spherical monomers. In this study, the diffusion-limited particle-cluster aggregation (DLPCA) algorithm[13] is used to generate aggregated BC, where identical spherical monomers are added iteratively. And each step exactly satisfies the following statistical scaling law:

$$N = k_{\rm f}(R_{\rm g}/a)^{D_{\rm f}}, \quad (8)$$

where a is the mean radius of spherical monomer, $k_{\rm f}$ is the fractal prefactor, $D_{\rm f}$ is the fractal dimension, N is the monomer number of the aggregates, and $R_{\rm g}$ is the radius of gyration. The usual $R_{\rm g}$ is defined via the mean square of the distances between the spherical monomer center and the geometrical center of mass of the aggregate. From the step $N-1$ to N, the center position $\boldsymbol{r}_N$ of the N-th monomer must be situated on the surface of the currently existing aggregate determined by the equation

$$(\boldsymbol{r}_N-\boldsymbol{r}_{N-1}^{0})^2 = \frac{N^2a^2}{N-1}\left(\frac{N}{k_{\rm f}}\right)^{2/D_{\rm f}}-\frac{Na^2}{N-1} - Na^2\left(\frac{N-1}{k_{\rm f}}\right)^{2/D_{\rm f}}, \quad (9)$$

where $\boldsymbol{r}_{N-1}^{0}$ is the center of mass of the first $N-1$ monomers. The center positions of monomers as input parameters for GMM will be used to calculate the scattering properties of particles.

3. Results

3.1. Single coated dust (Group I)

Dust particles can provide reaction sites for heterogeneous chemical reactions and particle coagulations. Li and Shao found that about 90% of mineral dust particles were coated in the haze samples by analyzing TEM images.[10] In this paper, GMM method is employed to calculate the scattering properties of BC/OC/WS-coated dust (group I particles) at the wavelength of 1.6 μm. The mineral dust core is assumed to be a sphere (axial ratio $a/b = 1$) or spheroid ($a/b = 1.5$, which is the typical aspect ratio of Asian dust[14]), and its radius, $R_{\rm core}$, ranges from 0.1 μm to 1.5 μm because the long-range transport of dust causes a shift towards smaller size where the radius hereinafter is equal-volume sphere radius. The ratio of thickness, q varies from 0 to 0.2, which is the ratio of thickness of coating to the radius of dust core. Table 1 shows the complex refractive indices of different aerosol species from OPAC database.[15] Because haze events are always characterized by high relative humidity (RH), the refractive index of WS at an RH of 80% is selected.

Table 1. Complex refractive indices of transported dust, BC, OC, and WS (RH = 80%) in 1.6-μm wavelength.

	Dust (tran.)	BC	OC	WS (RH = 80%)
Real	1.53	1.778	1.487	1.391
Imaginary	5.6×10^{-3}	0.468	4.8×10^{-5}	8.53×10^{-3}

Figure 1 shows that the differences in scattering phase functions (SPFs) between sphere and spheroid for pure dust are smaller than those for coated dust. Both the particle shape and the chemical component of coating influence the SPFs. When the coating material, $R_{\rm core}$ and q are fixed, the scattering intensities of spheroidal group I particles are generally larger than those of spherical particles in the forward scattering direction, but they are smaller than those of spherical particles in the backward scattering direction. With the increase of $R_{\rm core}$, the SPFs of spheroidal group I particles increase for the scattering angles between 0° and 30°. For the scattering angles between 150° and 180°, the SPFs increase for spheroidal OC-coated particles, but decrease for the BC and WS-coated particles.

The results of extinction cross section ($C_{\rm ext}$), scattering cross section ($C_{\rm sca}$), absorption cross section ($C_{\rm abs}$), single scattering albedo (ω), and asymmetry factor (g) of group I particles with $R_{\rm core} = 1.0$ μm are given in Fig. 2. It is indicated that the scattering parameters are significantly changed by particle coatings, even when the q is only 0.02. For example, the ω of spheroidal BC-coated dust with $q = 0.02$ is only 0.473 due to the relatively strong light absorption of BC, while the ω of pure spheroidal dust reaches 0.972. The differences in $C_{\rm ext}$, $C_{\rm sca}$, $C_{\rm abs}$, and ω between sphere and spheroid become smaller for BC and WS-coated dusts when the q ranges from 0.02 to 0.2. These differences of BC-coated dust influenced by particle shape can be up to 4.22 μm^2, 7.42 μm^2, 3.22 μm^2, and 0.409 for $C_{\rm ext}$, $C_{\rm sca}$, $C_{\rm abs}$, and ω respectively.

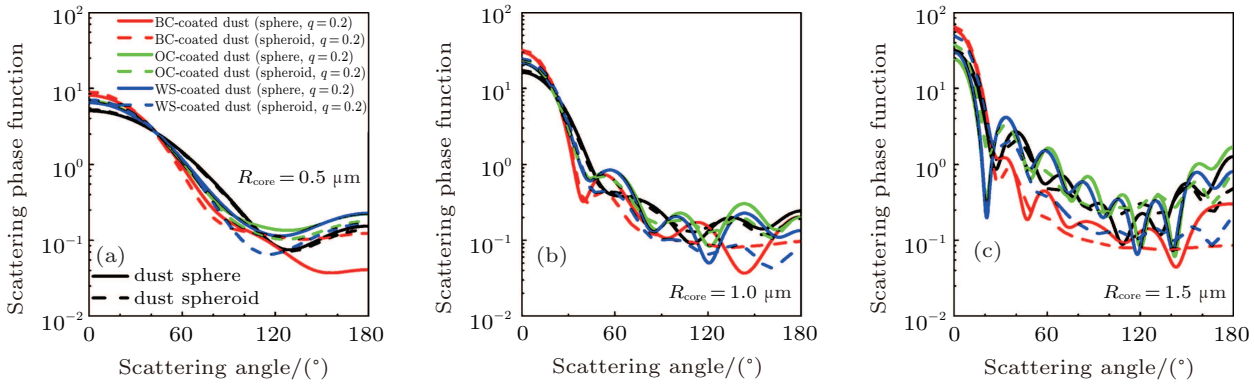


Fig. 1. (color online) Scattering phase functions of group I particles with $q = 0.2$ and pure dust in 1.6-μm wavelength for $R_{\rm core} = 0.5$, 1.0, and 1.5 μm.

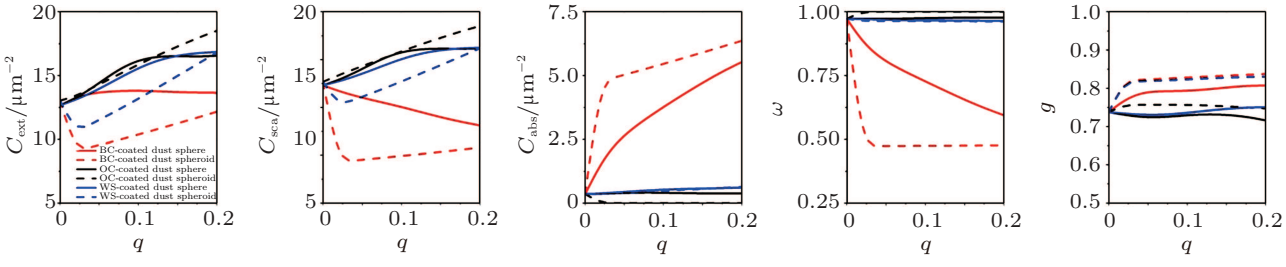


Fig. 2. (color online) Extinction cross sections, scattering cross sections, absorption cross sections, single scattering albedos, and asymmetry factors of spherical and spheroidal group I particles with $R_{\rm core} = 1.0$ μm in 1.6-μm wavelength.

3.2. Dust semi-externally mixed with other particles (Group II)

In the ambient air, dust semi-externally mixed with other particles (group II, a two-particle system) is another typical structure for polluted dust because dust particles are always subjected to collision with other particles. Here, we just take into account the two-sphere or two-spheroid system composed of two spherical or spheroidal ($a/b = 1.5$) monomers with the same size (Figs. 3(a) and 3(b)). One monomer is mineral dust, and the other is BC, or OC or WS. The SPFs of group II particles with the radius of dust monomer, $R_{\rm dust} = 0.5$, 1.0, and 1.5 μm are shown in Fig. 4. The scattering intensities of group II particles are mainly affected by the monomer size. The chemical component and shape of monomers have a relatively small effect on the SPFs in both forward and backward scattering directions.

Unlike SPF, the $C_{\rm ext}$, $C_{\rm sca}$, $C_{\rm abs}$, and ω of the two-sphere/spheroid system are closely related to the chemical properties of monomers (Fig. 5). When $R_{\rm dust} = 1.5$ μm, the $C_{\rm sca}$ for BC-dust two-spheroid system is only about half that for OC-dust one, while the $C_{\rm abs}$ for BC-dust one is 7 times that for OC-dust one. When $R_{\rm dust} = 0.5$ μm, the ω for BC-dust two-spheroid system is 0.265 smaller than that for OC-dust one, and it is 0.24 smaller than that for WS-dust one. Figure 5 also indicates that all of the $C_{\rm ext}$, $C_{\rm sca}$, $C_{\rm abs}$, ω, and g are insensitive to the shape of monomers.

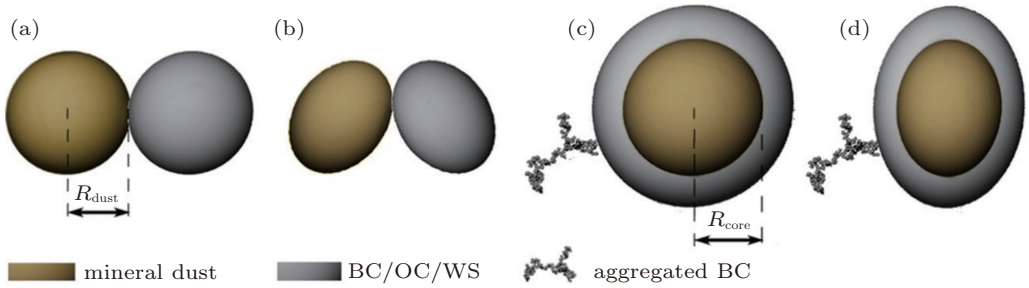


Fig. 3. (color online) Simulations of polluted dust particles. (a) and (b) Group II particles (two-sphere/spheroid system). (c) and (d) Group III particles with spherical/spheroidal host dust for $a = 15$ nm, $N = 100$, $D_{\rm f} = 1.82$, and $k_{\rm f} = 1.19$.

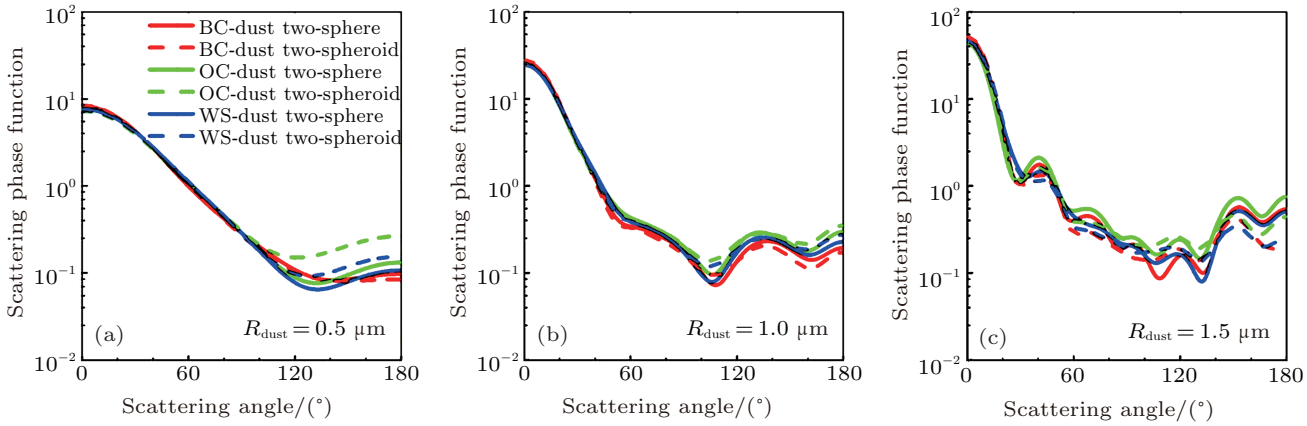


Fig. 4. (color online) Scattering phase functions of group II particles in 1.6-μm wavelength for $R_{\rm dust} = 0.5$, 1.0, and 1.5 μm.

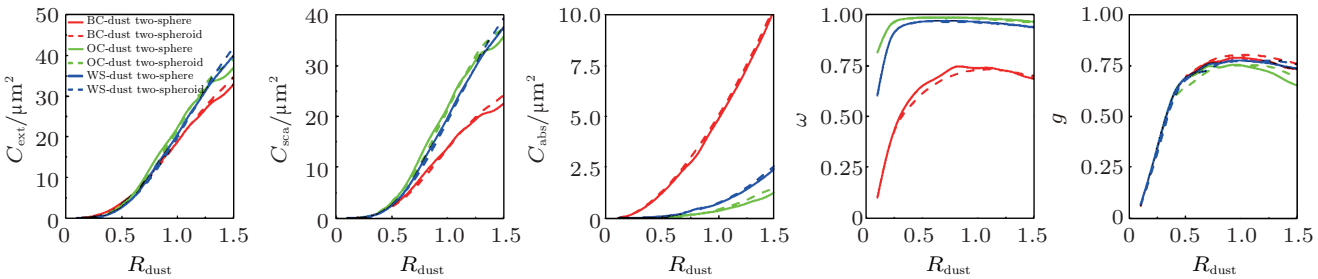


Fig. 5. (color online) Extinction cross sections, scattering cross sections, absorption cross sections, single scattering albedos, and asymmetry factors of group II particles in 1.6-μm wavelength.

3.3. Coated dust semi-externally mixed with aggregated BC (Group III)

For the group III particles, coated dust as the host particle is a spherical or spheroidal ($a/b = 1.5$) dust core with OC or WS coating. Aggregated BC is generated by the DLPCA algorithm. The monomer radius of BC aggregate, a, is fixed to be 15 nm, and the values of D_f and k_f are selected following the study by Sorensen and Roberts,[16] in which $D_f = 1.82$ and $k_f = 1.19$. Figures 3(c) and 3(d) show simulations of BC aggregates attached to spherical and spheroidal coated dusts respectively.

Figure 6 depicts the SPFs of OC/WS-coated dust semi-externally mixed with aggregated BC composed of different numbers of monomers. By comparing Fig. 6 with Fig. 1, it can be seen that the SPF of a group III particle is dominated by the shape and chemical component of the host dust. However, the attached BC aggregate has little effect on the SPF of the overall particle, and this effect tends to become smaller as the radius of dust core increases. It is suggested that the direction of light will not be strikingly changed by increasing the monomer number of the attached BC aggregate.

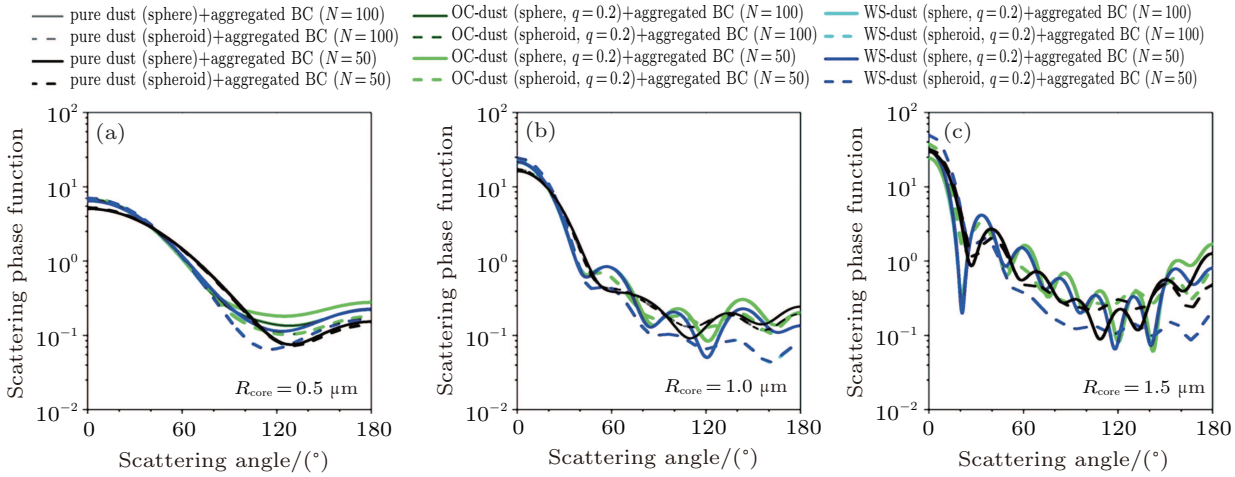


Fig. 6. (color online) Scattering phase functions of group III particles at 1.6-μm wavelength for $R_{core} = 0.5$, 1.0, and 1.5 μm.

Like SPF, the C_{ext}, C_{sca}, C_{abs}, ω, and g of group III particles are also significantly influenced by the chemical and morphological properties of the host dust, especially for large-size particles. The calculated results of group III particles with $N = 100$ are given in the top panels in Fig. 7. To investigate the effect of attached BC aggregate on the scattering properties of the overall group III particle, we subtract the scattering parameter of a group III particle with $N = 50$ from that of the

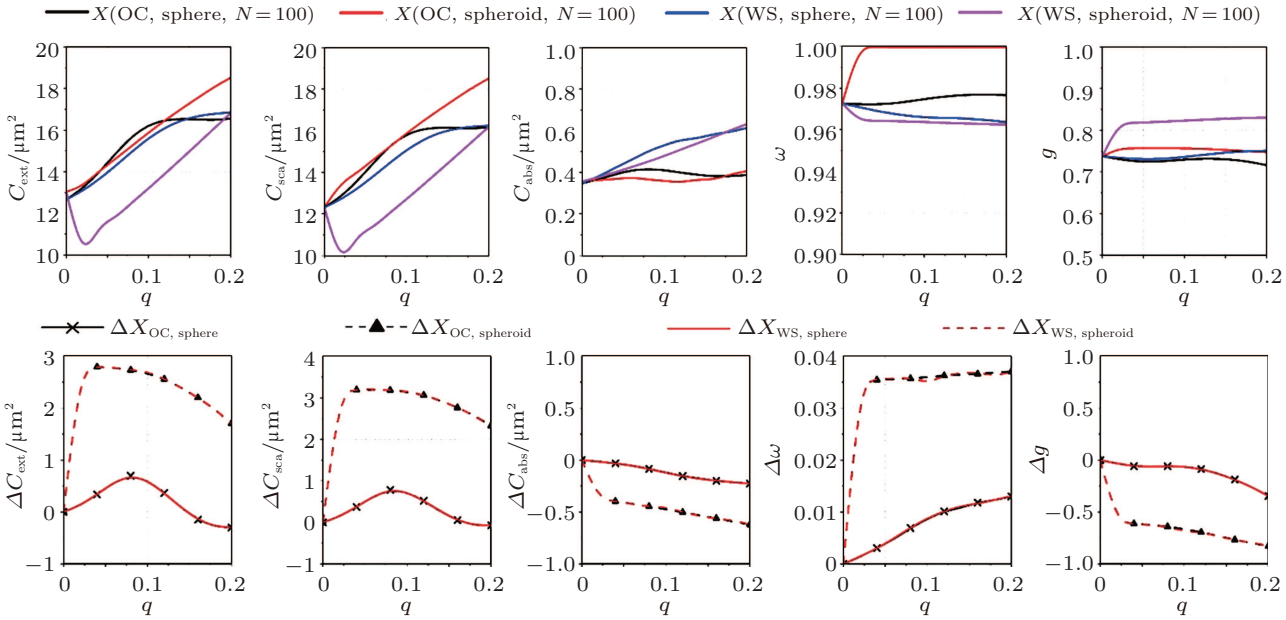


Fig. 7. Extinction cross sections, scattering cross sections, absorption cross sections, single scattering albedos, and asymmetry factors of group III particles with BC aggregates ($N = 100$) for $R_{core} = 1.0$ μm at 1.6-μm wavelength (top panels), and their corresponding differences of group III particles with different sized BC aggregates ($N = 50$ and 100), where X denotes any of these five scattering parameters.

corresponding particle with $N = 100$ (shown in the bottom panels in Fig. 7), and the difference is denoted as

$$\Delta X_{co,sh} = X(co, sh, N = 100) - X(co, sh, N = 50), \quad (10)$$

where X can be any of $C_{\rm ext}$, $C_{\rm sca}$, $C_{\rm abs}$, ω, and g, co is the chemical component of dust coating, and sh is the shape of coated dust. In general, the effect of BC aggregate on the scattering properties of overall particle is nearly independent of the chemical property of the host particle. And this effect for the spheroidal host particle is larger than that for the corresponding spherical one. When $q = 0.2$ and $R_{\rm core} = 1.0$ μm, the absolute values of $\Delta C_{\rm ext}$, $\Delta C_{\rm sca}$, $\Delta C_{\rm abs}$, $\Delta\omega$, and Δg for the group III particle with spheroidal dust are 1.7 μm^2, 2.32 μm^2, 0.62 μm^2, 0.037, and 0.083, respectively, while those for the group III particle with spherical dust are only 0.3 μm^2, 0.07 μm^2, 0.23 μm^2, 0.013, and 0.034 respectively.

4. Conclusion

The influences of particle size, morphology, and chemical composition on the scattering properties for three specific types of polluted dust in 1.6-μm wavelength are investigated in this study. Our analysis of numerical results demonstrates that the scattering characteristics of these internal mixtures and semi-external mixtures are significantly different from each other. For the coated dust particles, the coatings could significantly influence the results of $C_{\rm ext}$, $C_{\rm sca}$, $C_{\rm abs}$, and ω, even when the thickness values of coatings are very small. For the two-particle system, the scattering properties of overall particle are affected mainly by the size and chemical component of the monomers, and next by the monomer shape. For the coated dust semi-externally mixed with aggregated BC, the coated dust as the host particle controls the optical characteristics of the overall particles. Therefore, the internally and semi-externally mixed polluted dust should be properly modeled in the CO_2 retrieval, and other remote sensing and radiation balance applications.

References

[1] Chevallier F, Bréon F M and Rayner P J 2007 *J. Geophys. Res.* **112** D09307
[2] Aben I, Hasekamp O and Hartmann W 2007 *J. Quantum Spectrosc. Radiat. Transfer* **104** 450
[3] Ma J, Chen Y, Wang W, Yan P, Liu H, Yang S, Hu Z and Lelieveld J 2010 *J. Geophys. Res.* **115** D18204
[4] Li S, Chen L, Xiong X, Tao J, Su L, Han D and Liu Y 2013 *IEEE Trans. Geosci. Remote Sens.* **51** 2528
[5] Pósfai M, Axisa D, Tompa É, Freney E, Bruintjes R and Buseck P R 2013 *Atmos. Res.* **122** 347
[6] Mishchenko M I, Travis L D and Mackowski D W 1996 *J. Quantum Spectrosc. Radiat. Transfer* **55** 535
[7] Yang P and Liou K N 1995 *J. Opt. Soc. Am. A* **12** 162
[8] Purcell E M and Pennypacker C R 1973 *Astrophys. J.* **186** 705
[9] Xu Y L and Gustafson B Å S 2001 *J. Quantum Spectrosc. Radiat. Transfer* **70** 395
[10] Li W J and Shao L Y 2009 *Atmos. Chem. Phys.* **9** 1863
[11] Chou C, Formenti P, Maille M, Ausset P, Helas G, Harrison M and Osborne S 2008 *J. Geophys. Res.* **113** D00C10
[12] Arimoto R, Kim Y J, Kim Y P, Quinn P K, Bates T S and Anderson T L, *et al.* 2006 *Global. Planet. Change* **52** 23
[13] Filippov A V, Zurita M and Rosner D E 2000 *J. Colloid. Interface Sci.* **229** 261
[14] Parungo F 1996 *Science and Technology Corporation Technical Report for NOAA*
[15] Hess M, Koepke P and Schult I 1998 *Bull. Am. Meteor. Soc.* **79** 831
[16] Sorensen C M and Roberts G C 1997 *J. Colloid. Interface Sci.* **186** 447